EJNMMI Radiopharmacy and Chemistry

RESEARCH ARTICLE Open Access

Mitochondria-tropic radioconjugates to enhance the therapeutic potential of terbium-161

Joana F. Santos[1], Camille Van Laere[2,3], Catarina D. Silva[1], Irwin Cassells[2,3], Célia Fernandes[1,4], Paula Raposinho[1,4], Ana Belchior[1,4], Catarina I. G. Pinto[1], Filipa Mendes[1,4], Christopher Cawthorne[5], Maarten Ooms[2], Michiel Van de Voorde[2], Frederik Cleeren[3*] and António Paulo[1,4*]

*Correspondence:
Frederik Cleeren
frederik.cleeren@kuleuven.be
António Paulo
apaulo@ctn.tecnico.ulisboa.pt
[1]C2TN - Centro de Ciências e Tecnologias Nucleares, Instituto Superior Técnico, Universidade de Lisboa, Bobadela LRS 2695-066, Portugal
[2]Nuclear Medical Applications, Belgian Nuclear Research Centre (SCK CEN), Mol, Belgium
[3]Laboratory for Radiopharmaceutical Research, Department of Pharmaceutical and Pharmacological Sciences, University of Leuven, Leuven B-3000, Belgium
[4]DECN - Departamento de Engenharia e Ciências Nucleares, Instituto Superior Técnico, Universidade de Lisboa, Bobadela LRS 2695-066, Portugal
[5]Nuclear Medicine and Molecular Imaging, Department of Imaging and Pathology, University of Leuven, Leuven, Belgium

Abstract

Background Strategies that focus on delivering Auger electron emitters to highly radiosensitive intracellular targets—such as the nucleus, cell membrane, or mitochondria—are gaining attention. Targeting these organelles could enhance therapeutic efficacy while minimizing off-target toxicity by allowing lower administered doses. In this context, this study explores the therapeutic potential of ^{161}Tb-labeled radiocomplexes that integrate the mitochondria-targeting triphenylphosphonium (TPP) moiety with a prostate-specific membrane antigen (PSMA) targeting vector. The goal is to assess these dual-targeted radiocomplexes for their ability to deliver conversion electrons (CE) and Auger electrons (AEs) to prostate cancer (PCa) cells, specifically targeting the mitochondria to enhance therapeutic efficacy.

Results Two novel radiocomplexes, [^{161}Tb]Tb-TPP-PSMA and [^{161}Tb]Tb-TPP-G_3-PSMA, were synthesized with high radiochemical yield and purity. The proposed structures were validated using HPLC and ESI-MS analysis, with their ^{nat}Tb counterparts serving as reference compounds. In vitro experiments included cellular uptake, internalization, mitochondrial uptake, and DNA damage assays in PSMA-positive PCa cell lines. Clonogenic assays were performed to evaluate cell survival post-treatment. In vivo studies were conducted using SCID/Beige mice bearing PCa xenografts and involved µSPECT/CT imaging and radiometabolite analysis to evaluate biodistribution, pharmacokinetics, tumor uptake and in vivo stability of the radiocomplexes. Both [^{161}Tb]Tb-TPP-PSMA and [^{161}Tb]Tb-TPP-G_3-PSMA showed high radiochemical stability and were efficiently internalized by PSMA-positive cells, while showing minimal uptake in PSMA-negative cells. These dual-targeted radiocomplexes demonstrated significantly higher mitochondrial uptake compared to the non-TPP-containing [^{161}Tb]Tb-PSMA-617, leading to increased DNA damage and enhanced radiocytotoxicity. In vivo, the dual-targeted complexes demonstrated PSMA-specific tumor uptake and pharmacokinetics comparable to [^{161}Tb]Tb-PSMA-617, with effective clearance from non-target tissues.

Springer Open

© The Author(s) 2025. **Open Access** This article is licensed under a Creative Commons Attribution-NonCommercial-NoDerivatives 4.0 International License, which permits any non-commercial use, sharing, distribution and reproduction in any medium or format, as long as you give appropriate credit to the original author(s) and the source, provide a link to the Creative Commons licence, and indicate if you modified the licensed material. You do not have permission under this licence to share adapted material derived from this article or parts of it. The images or other third party material in this article are included in the article's Creative Commons licence, unless indicated otherwise in a credit line to the material. If material is not included in the article's Creative Commons licence and your intended use is not permitted by statutory regulation or exceeds the permitted use, you will need to obtain permission directly from the copyright holder. To view a copy of this licence, visit http://creativecommons.org/licenses/by-nc-nd/4.0/.

Conclusions The TPP-modified ^{161}Tb-radiocomplexes effectively targeted the mitochondria of PSMA-positive PCa cells, leading to increased DNA damage and reduced cell viability compared to single-targeted radiocomplexes. These findings suggest that dual-targeting strategies, which combine PSMA and mitochondrial targeting, can enhance the therapeutic potential of radiopharmaceuticals for prostate cancer treatment.

Keywords ^{161}Tb-radiocomplexes, PSMA, Mitochondria, Prostate cancer, Auger electrons

Introduction

Lutetium-177 (^{177}Lu) has emerged as a pivotal radionuclide in the development of cancer theranostics, achieving significant success with ^{177}Lu-labeled peptides or peptidomimetics, particularly those targeting somatostatin (SST) receptors or prostate specific membrane antigens (PSMA). These advancements led to the FDA and EMA approval of [^{177}Lu]Lu-DOTA-TATE (Lutathera™) and [^{177}Lu]Lu-PSMA-617 (Pluvicto™) for targeted radionuclide therapy (TRT) of metastatic or unresectable neuroendocrine neoplasms (NEN) and metastatic castration resistant prostate cancer (PCa), respectively (Ruigrok et al. 2019; Rasul et al. 2020). While ^{177}Lu ($T_{1/2}$ = 6.65 d) remains a widely used soft β^- emitter, the emerging radionuclide terbium-161 (^{161}Tb, $T_{1/2}$ = 6.96 d) presents a compelling alternative due to its emission of conversion electrons (CE) and Auger electrons (AE), which offer enhanced therapeutic potential, as demonstrated by numerous preclinical studies (Bolcaen et al. 2023; Laere et al. 2024; Müller et al. 2019; Borgna et al. 2022; Favaretto et al. 2023; Tschan et al. 2023; Holzleitner et al. 2024; Spoormans et al. 2024; Collins et al. 2022).

Compared to β^- particles, CEs and AEs exhibit a higher linear energy transfer (LET), with AEs delivering energy over a nanometric range (< 500 nm), making them particularly effective for targeting micrometastases and single cancer cells. This capability is critical for preventing recurrence and disease progression, which is hardly achieved with conventional β^- emitters like ^{177}Lu due to the longer tissue penetration and reduced efficacy of β^- particles in small lesions (Larouze et al. 2023).

To exploit the potential of AEs, strategies that focus on delivering AE emitters to highly radiosensitive intracellular targets—such as the nucleus, cell membrane, or mitochondria—are gaining traction. Targeting these organelles could enhance therapeutic efficacy while minimizing off-target toxicity by allowing lower administered doses (Bolcaen et al. 2023).

Our research focuses on mitochondrial targeting to enhance radiobiological effects of AE-emitters. Mitochondria, essential extranuclear organelles, are highly vulnerable to ionizing radiation (IR) due to their limited DNA repair capacity and their role in reactive oxygen species (ROS) generation. IR-induced mitochondrial damage can compromise cellular respiration, induce oxidative stress, and trigger apoptotic pathways, making them a promising target for AE-emitting radionuclides (Averbeck and Rodriguez-Lafrasse 2021). Towards this goal, we have considered radioconjugates carrying the triphenylphosphonium (TPP) group as a mitochondrion-tropic pharmacophore. Due to their delocalized cationic nature, TPP derivatives preferentially accumulate in mitochondria, driven by the organelle's negative transmembrane potential (Zielonka et al. 2017).

Despite their potential, studies on mitochondrion-tropic radioconjugates for AE-based-TRT remain limited. Notably, ^{99m}Tc-complexes combining a TPP pharmacophore with a bombesin (BBN) derivative have been reported (Fernandes et al. 2022; Figueiredo et al. 2021). More recently, we reported on the ^{111}In-radiocomplexes [^{111}In]In-TPP-PSMA and [^{111}In]In-TPP-G_3-PSMA, featuring DOTA-based chelators functionalized with a PSMA inhibitor and a TPP group (Santos et al. 2024). These dual-targeted ^{111}In-complexes outperformed the single-targeted [^{111}In]In-PSMA-617, showing a greater efficacy in compromising the survival of PSMA-positive PCa cells while retaining a similar tumor-targeting ability in mice with PSMA-positive PCa xenografts (Santos et al. 2024).

Although indium-111 (^{111}In; $T_{1/2}$= 2.80 d) is an AE emitter, its potential for AE TRT of cancer is limited compared to ^{161}Tb, primarily due to its less favorable photon-to-electron (p/e) energy ratio per decay (^{111}In, p/e = 11.6; ^{161}Tb, p/e = 0.18) (Bolcaen et al. 2023). Building on our promising results with dual-targeting ^{111}In-radiocomplexes, we extended our research to investigate the potential of TPP-containing ^{161}Tb-radiocomplexes to leverage the potent AE emitting properties of ^{161}Tb for TRT, through the specific targeting of the mitochondria of PSMA-positive cancer cells (Fig. 1).

In this study we synthesized and evaluated two dual-targeted ^{161}Tb complexes: [^{161}Tb]Tb-TPP-PSMA and [^{161}Tb]Tb-TPP-G_3-PSMA. Notably, the [^{161}Tb]Tb-TPP-G_3-PSMA complex contains a cathepsin B-cleavable gly-gly-gly (G_3) linker between the PSMA unit and the DOTA chelator framework. Previous in vitro studies with ^{99m}Tc- and ^{225}Ac-radioconjugates carrying G_3 linkers demonstrated efficient cleavage of this tri-amino acid linker by cathepsin B (Figueiredo et al. 2021; Antczak et al. 2006), a lysosomal cysteine protease frequently overexpressed in cancer cells and implicated in tumor invasion and metastasis (Xie et al. 2023).

We hypothesized that cleavage of the G_3 linker would release a smaller TPP-containing radiocomplex with enhanced ability to reach the mitochondria of prostate cancer

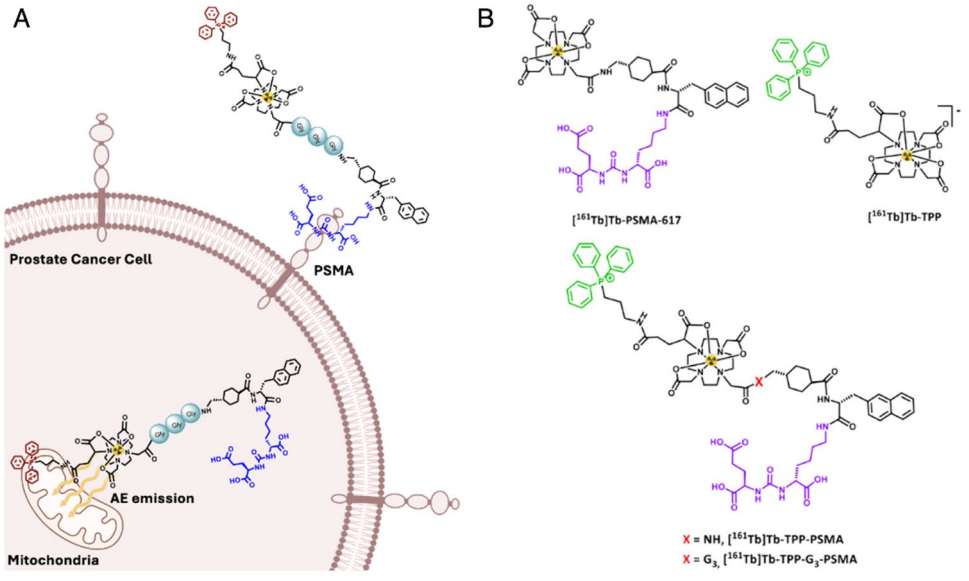


Fig. 1 (**A**) Schematic representation of the delivery of a TPP-containing ^{161}Tb-complex to the mitochondria of PSMA-positive PCa cells. (**B**) Molecular structures of the single- and dual-targeted ^{161}Tb-complexes evaluated in this study, including a dual-targeted complex carrying a cathepsin B cleavable gly-gly-gly (G_3) linker

cells following endosomal or lysosomal escape. By targeting mitochondria, these ^{161}Tb-radioconjugates are designed to maximize the therapeutic efficacy of AE emissions.

Here, we present the preclinical evaluation of these novel mitochondria-targeting ^{161}Tb-radioconjugates in both cellular and animal models of PCa. This innovative approach aims to fully leverage the unique radiobiological effects of AEs, providing a promising strategy to enhance TRT. We anticipate that this work will pave the way for novel therapeutic applications of ^{161}Tb-based radioconjugates in cancer treatment.

Materials and methods

Chemistry and radiochemistry

[^{161}Tb]$TbCl_3$ was produced at the Belgian Nuclear Research Centre (SCK CEN) using the previously described method(Cassells et al. 2021). Details on the synthesis and characterization of the different ^{161}Tb-radiocomplexes and their congeners with ^{nat}Tb are provided in the Supporting Information (SI), as well as the determination of the lipophilicity and in vitro stability studies (in PBS and cell culture medium) for the ^{161}Tb compounds.

Cellular studies

Cell uptake, internalization and mitochondrial uptake

Cellular uptake and internalization assays were performed for [^{161}Tb]Tb-TPP, [^{161}Tb]Tb-PSMA-617, [^{161}Tb]Tb-TPP-PSMA, and [^{161}Tb]Tb-TPP-G_3-PSMA using both PSMA-positive (LNCaP and PC3 PIP (PC3 transfected with PSMA)) and PSMA-negative (PC3 and PC3 flu) cell lines. Cells seeded in 24-well plates were incubated at 37 °C with approximately 7.4 kBq of the radiocomplexes for 5 min to 4 h. To confirm PSMA specificity, blockade experiments were performed in PSMA-positive cells using the PSMA inhibitor 2-(phosphonomethyl)pentanedioic acid (2-PMPA) (100 μM/well). Cellular retention of the PSMA-targeted complexes was assessed in PC3 PIP cells, following a 3 h incubation with approximately 7.4 kBq of radiocomplexes at 37 °C. Efflux was measured by monitoring radioactivity released into fresh culture media over 5 h. For mitochondrial uptake, PC3 PIP cells in a T75 culture flask were incubated with approximately 7.4 MBq of the radiocomplexes [^{161}Tb]Tb-PSMA-617, [^{161}Tb]Tb-TPP-PSMA or [^{161}Tb]Tb-TPP-G_3-PSMA for 1 h at 37 °C. Mitochondrial fractions were isolated using the Human Mitochondria Isolation Kit (Miltenyi Biotec) following the manufacturer's protocol. Detailed experimental procedures, as previously described (Santos et al. 2024; Rogakou et al. 1998), are provided in the Supplementary Information (SI).

Clonogenic and γ–H2AX assays

The radiobiological effects of the different PSMA-targeted complexes ([^{161}Tb]Tb-PSMA-617, [^{161}Tb]Tb-TPP-PSMA, and [^{161}Tb]Tb-TPP-G_3-PSMA) in the PC3 PIP cell line were evaluated using clonogenic and γ–H2AX assays, as detailed in the SI and previously described protocols (Fernandes et al. 2022; Santos et al. 2024). For the clonogenic assay, 200 PC3 PIP cells, seeded in a 6 well-plates, were exposed to radiolabeled complexes (0.037–1.85 MBq) for 4 h at 37 °C. After incubation, the treatment solution was removed, and fresh medium was added to allow colony formation over 10 days. For γ-H2AX assay, 1×10^4 PC3 PIP cells previously seeded in an eight-well chamber slide were incubated with radiolabeled complexes (0.185, 0.37 and 0.74 MBq) for 2 and 4 h at

37 °C. γ–H2AX immunofluorescence assay was performed immediately after incubation, or following a 24 h period to allow for DNA damage repair (for the 4 h of incubation).

Animal studies

All animal procedures were approved by the KU Leuven ethical review board (ethical approval reference P200/2021) and were carried out in accordance with Directive 2010/63/EU. μSPECT imaging studies were performed in female SCID/Beige mice (Charles River, St Germain Nuelles, France) engrafted with PSMA-positive tumors (using PC3 PIP cells) and PSMA-negative tumors (using PC3 flu cells). Xenografted mice (4 animals per group) were injected with [^{161}Tb]Tb-PSMA-617, [^{161}Tb]Tb-TPP-PSMA and [^{161}Tb]Tb-TPP-G_3-PSMA. The in vivo stability of [^{161}Tb]Tb-TPP-G_3-PSMA was also assessed in the same animal model. After excision, PSMA-positive and PSMA-negative tumors were analyzed by autoradiographic methods. Details on the different animal studies are given in the SI.

Statistical analysis

Quantitative data are expressed as mean ± standard deviation, unless stated otherwise. For comparison of results, the means were compared using a mixed model ANOVA analysis in GraphPad Prism 9.3.1, corrected using Sidak's or Tukey multiple comparison test. Values were determined to be statistically significant for p-values less than the threshold value of 0.05.

Results

Radiolabeling and radiochemical stability

The different ^{161}Tb-radiocomplexes ([^{161}Tb]Tb-PSMA-617, [^{161}Tb]Tb-TPP-PSMA, [^{161}Tb]Tb-TPP-G_3-PSMA and [^{161}Tb]Tb-TPP) were synthesized with high radiochemical yield (RCY > 95%) and a molar activity of 5–20 MBq/nmol by reacting $^{161}TbCl_3$ with the respective precursors (Figure S1) at 95 °C for 15 min, using a final ligand concentration of 10 μM. All batches of ^{161}Tb-complexes were subjected to purification using solid phase extraction (SPE) chromatography to remove residual contaminants, such as free metal ions and insoluble terbium hydroxides, and to ensure consistent radiochemical purity across all samples tested in biological assays. After purification, all radiocomplexes exhibited high radiochemical purity (> 98%), as confirmed by radio-HPLC analysis. Their chemical identity was ascertained by HPLC co-injection and ESI-MS experiments with the ^{nat}Tb counterparts as described in the SI (Figs. S2-S5). Additionally, the characterization of the ^{161}Tb-complexes included an assessment of their lipophilicity based on the determination of their partition coefficients (Table S1). All complexes were found to be hydrophilic, with Log $D_{pH\ 7.4}$ values ranging from − 2.75 ± 0.09 to -2.35 ± 0.02, and following the order: [^{161}Tb]Tb-TPP-G_3-PSMA < [^{161}Tb]Tb-PSMA-617 < [^{161}Tb]Tb-TPP < [^{161}Tb]Tb-TPP-PSMA (Table S2).

The radiochemical stability of ^{161}Tb-radiocomplexes (10–20 MBq/mL) in PBS and cell culture medium was evaluated over a 24-hour period at 37 °C using radio-HPLC (Figs. S6-S9). No degradation products or shift in retention times were observed, confirming their excellent in vitro stability.

Cellular studies

Cellular uptake and internalization

The cellular internalization and surface-bound fractions as well as the total uptake (internalization + surface-bound) of [^{161}Tb]Tb-PSMA-617, [^{161}Tb]Tb-TPP-PSMA, [^{161}Tb]Tb-TPP-G_3-PSMA and [^{161}Tb]Tb-TPP were evaluated for up to 4 h in prostate cancer cells with different levels of PSMA expression, as determined by western blot analysis (Fig. S10): PC3 PIP (PSMA+) and PC3 flu (PSMA-) cells (Fig. 2A and Fig. S11), LNCaP (PSMA+) and non-modified PC3 (PSMA-) cells (Fig. S12).

An initial assay was conducted in the PC3 PIP and flu cell lines to evaluate the PSMA-targeting ability of the complexes. The results showed that the three PSMA-targeting complexes exhibited high, time-dependent total uptake, in contrast to [^{161}Tb]Tb-TPP (Fig. S11). Interestingly, after 4 h of incubation, the uptake of [^{161}Tb]Tb-PSMA-617 and [^{161}Tb]Tb-TPP-PSMA was significantly higher (90.8% and 91.1%, respectively; $p < 0.0001$) compared to [^{161}Tb]Tb-TPP-G_3-PSMA (64.5%). This difference is further reflected in the lower portion of surface-associated activity for [^{161}Tb]Tb-TPP-G_3-PSMA (40.0%) compared to [^{161}Tb]Tb-TPP-PSMA and [^{161}Tb]Tb-PSMA-617 (62.7% and 68.2%, respectively; $p < 0.0001$) (Fig. S11). However, despite these differences, [^{161}Tb]Tb-PSMA-617, [^{161}Tb]Tb-TPP-PSMA and [^{161}Tb]Tb-TPP-G_3-PSMA presented similar cellular internalization profiles in PSMA-positive PC3 PIP cells with internalization values ranging from 22.6 to 28.3% after 4 h of incubation (Fig. 2A).

Due to the considerably lower PSMA expression level in LNCaP cells compared to PC3 PIP cells, the total uptake, surface-bound and internalization of PSMA-bearing complexes were 7- to 12-fold lower in LNCaP cells (Fig. S12). Nevertheless, the [^{161}Tb]Tb-PSMA-617, [^{161}Tb]Tb-TPP-PSMA and [^{161}Tb]Tb-TPP-G_3-PSMA complexes exhibited similar internalization profiles in LNCaP cells, with 3.4–4.0% of the applied activity internalized in the cells after 4 h incubation (Fig. S12). For [^{161}Tb]Tb-TPP-PSMA and [^{161}Tb]Tb-TPP-G_3-PSMA these data correspond to 56.3% and 50.2% of the cell associated activity, respectively, which are quite similar to the corresponding values found for these dual targeted complexes in PC3 PIP cells (50.7% and 48.7%, respectively). These

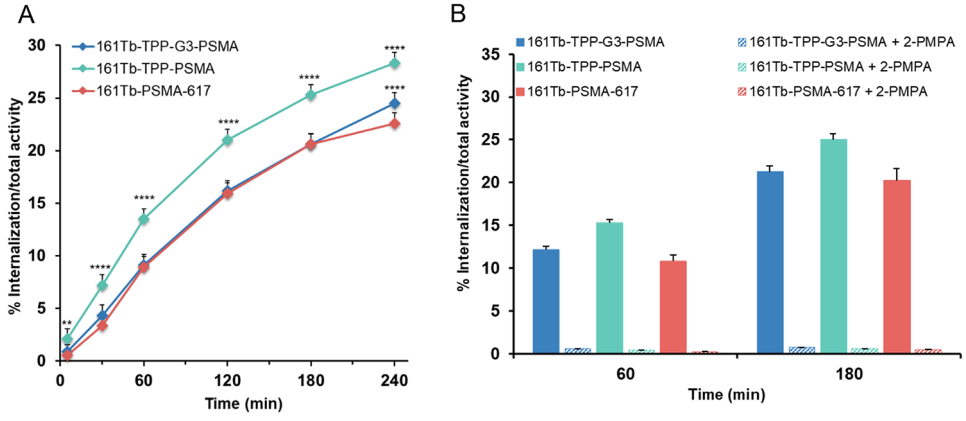


Fig. 2 Cellular binding of [^{161}Tb]Tb-TPP-G_3-PSMA, [^{161}Tb]Tb-TPP-PSMA and [^{161}Tb]Tb-PSMA-617 in PC3 PIP cells. (**A**) Time-dependent internalization at 37 °C, expressed as a percentage of the total applied activity. (**B**) PSMA-blocking study: internalization of the radiocomplexes without or with 2-PMPA at 60 min and 180 min. Results were calculated from independent biological replicates ($n = 4$), and are given as the mean ± standard deviation (SD). The statistical difference for each time-point with respect to [^{161}Tb]Tb-PSMA-617 was assessed by two-way ANOVA with Tukey's multiple comparisons test (* $p < 0.05$; ** $p < 0.01$; **** $p < 0.001$)

findings indicate that the PSMA-binding capacity is not compromised by introducing the mitochondrion-tropic TPP and G_3 linker.

The cell surface binding and internalization of all complexes were strongly reduced in PC3 PIP cells following PSMA-blocking by co-incubation with the structurally unrelated PSMA inhibitor 2-(phosphonomethyl)pentanedioic acid (2-PMPA) (Fig. 2B and Fig. S13). The reduction in internalization exceeded 90% for all evaluated time points (Fig. S13D), implying that internalization is mediated through a PSMA-specific mechanism. In accordance, all PSMA-targeted complexes exhibited negligible cellular uptake in PSMA-negative PC3 and PC3 flu cells. Notably, [^{161}Tb]Tb-TPP, lacking the PSMA-targeting vector, displayed minimal uptake across all tested cell lines (PC3 PIP, PC3 flu, LNCaP and PC3) (Figs. S11-S12).

Efflux rate and mitochondrial uptake

All three radiocomplexes [^{161}Tb]Tb-PSMA-617, [^{161}Tb]Tb-TPP-PSMA and [^{161}Tb]Tb-TPP-G_3-PSMA, demonstrated considerable cellular internalization in PSMA-positive cells. To investigate their behavior further, efflux and mitochondrial uptake assays were performed using the PC3 PIP cell line. In general, [^{161}Tb]Tb-PSMA-617 and [^{161}Tb]Tb-TPP-PSMA exhibited similar efflux profiles, whereas [^{161}Tb]Tb-TPP-G_3-PSMA displayed significantly less retention of the internalized radioconjugate over the same period (Fig. 3A). Specifically, after 1 h of incubation, [^{161}Tb]Tb-PSMA-617 and [^{161}Tb]Tb-TPP-PSMA retained 84% and 87% of the applied activity, respectively, while [^{161}Tb]Tb-TPP-G_3-PSMA retained 75%. At 5 h post-incubation, the cell associated activity was 74% and 76% for the former two compounds, compared to 58% for the latter. These values remained relatively stable even after 24 h of incubation (data not shown).

In contrast, after 1 h of incubation with the tested compounds, the TPP-containing radiocomplexes ([^{161}Tb]Tb-TPP-PSMA and [^{161}Tb]Tb-TPP-G_3-PSMA) displayed

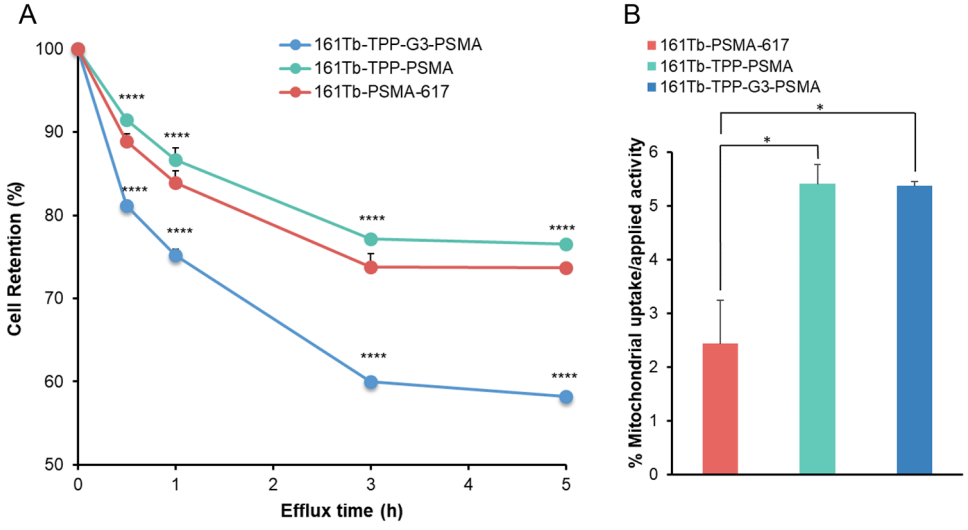


Fig. 3 Efflux and subcellular localization for [^{161}Tb]Tb-TPP-G_3-PSMA, [^{161}Tb]Tb-TPP-PSMA and [^{161}Tb]Tb-PSMA-617 in PC3 PIP cells. (**A**) Time-dependent cell retention, after prior incubation for 3 h at 37 °C. Results are expressed as a percentage of the initial internalized activity and were calculated from independent biological replicates (mean ± SD; $n = 4$). (**B**) Mitochondrial uptake in PC3 PIP cells at 37 °C after 1 h incubation expressed as a percentage of applied activity. Results were calculated from independent biological replicates (mean ± SD $n = 2$). The statistical difference for each time-point with respect to the [^{161}Tb]Tb-PSMA-617 was assessed by two-way ANOVA with Tukey's multiple comparisons test (* $p < 0.05$; **** $p < 0.001$)

a similarly higher mitochondrial uptake (5.4 ± 0.4% and 5.4 ± 0.1% of applied activity, respectively) compared to [^{161}Tb]Tb-PSMA-617 (2.4 ± 0.8% % of applied activity) ($p < 0.05$) (Fig. 3B).

Evaluation of radiobiological effects

To assess the effect of the radiocomplexes on cell survival, clonogenic assays were performed in PC3 PIP cells. This included the PSMA-targeted complexes ([^{161}Tb]Tb-PSMA-617, [^{161}Tb]Tb-TPP-PSMA and [^{161}Tb]Tb-TPP-G_3-PSMA) as well as [^{161}Tb]Tb-TPP. The cells were exposed to increasing activities of the radiocomplexes (0-1.85 MBq) during 4 h at 37 °C.

The PSMA-targeted complexes demonstrated a dose-dependent reduction in cell survival, whereas [^{161}Tb]Tb-TPP did not affect survival across all tested activities (Fig. 4), consistent with its negligible cellular uptake.

For applied activities of 0.185 MBq and higher, the TPP-containing dual-targeted complexes, [^{161}Tb]Tb-TPP-PSMA and [^{161}Tb]Tb-TPP-G_3-PSMA, showed a greater overall effect on the survival compared to [^{161}Tb]Tb-PSMA-617 (Fig. 4). In particular, using 0.185 MBq, the TPP-containing complexes reduced cell survival by 21 to 28%, while [^{161}Tb]Tb-PSMA-617 caused only an 8% reduction. Increasing the applied activity to 1.85 MBq further decreased cell survival by 69 and 82% for the TPP-containing complexes, compared to 26% for [^{161}Tb]Tb-PSMA-617. Furthermore, for the intermediate activities 0.37 and 0.74 MBq, [^{161}Tb]Tb-TPP-G_3-PSMA was significantly ($p = 0.0091$ and $p = 0.0006$, respectively) more effective to reduce cell survival than the [^{161}Tb]Tb-TPP-PSMA. Clonogenic assays performed on PSMA-negative PC3 flu cells showed that neither [^{161}Tb]Tb-TPP-PSMA nor [^{161}Tb]Tb-TPP-G_3-PSMA had affected cell survival for all the tested activities (Fig S14).

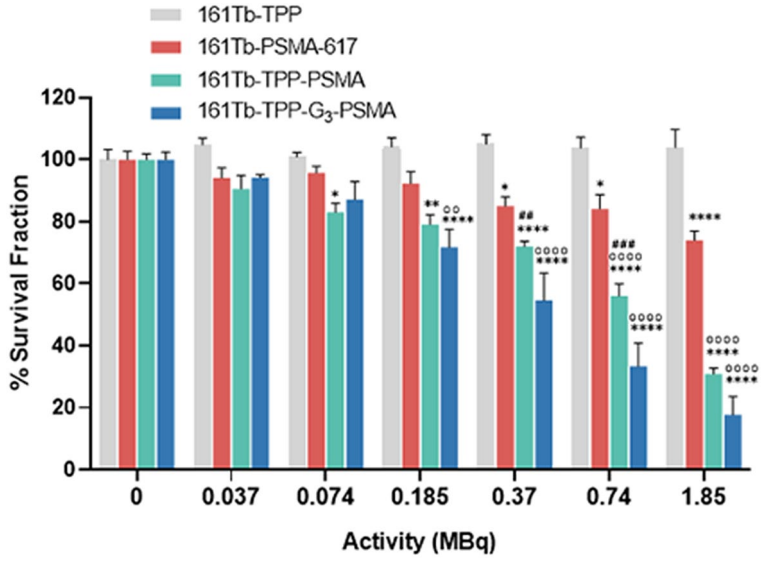


Fig. 4 Cellular survival fractions after 4 h incubation of PC3 PIP cells with 0-1.85 MBq of [^{161}Tb]Tb-TPP-G_3-PSMA, [^{161}Tb]Tb-TPP-PSMA, [^{161}Tb]Tb-PSMA-617 and [^{161}Tb]Tb-TPP, at 37 °C. Data correspond to mean ± SD ($n = 3$ replicates, 2–3 independent experiments). The statistical differences with respect to the control (0 MBq) (* $p < 0.05$; ** $p < 0.01$; **** $p < 0.001$) and to [^{161}Tb]Tb-PSMA-617 ($^{oo}p < 0.01$; $^{oooo}p < 0.001$), and between [^{161}Tb]Tb-TPP-PSMA and [^{161}Tb]Tb-TPP-G_3-PSMA ($^{\#\#}p < 0.01$; $^{\#\#\#}p < 0.005$) were assessed by two-way ANOVA with Tukey's multiple comparisons test

DNA damage evaluation

After evaluating the effect of the PSMA-targeted ^{161}Tb complexes on cell survival, their ability to cause DNA damage was assessed using the γ-H_2AX assay to quantify double-stranded DNA breaks (DSBs) through the quantification of γ-H_2AX foci (Rogakou et al. 1998). PC3 PIP cells were incubated with three different activities (0.185, 0.37 and 0.74 MBq) of the radiocomplexes for 2 and 4 h. For all conditions, the radiocomplexes caused a significant increase in the average foci number per nucleus when compared with the control condition, i.e. cells incubated with medium (Fig. 5 and Fig. S15).

The dual targeting complexes induced more extensive DNA damage than [^{161}Tb]Tb-PSMA-617, which is more evident for [^{161}Tb]Tb-TPP-G_3-PSMA, and in agreement with the survival results. For instance, [^{161}Tb]Tb-TPP-G_3-PSMA induced a significantly higher average number of foci per nucleus after incubation with 0.74 MBq for 4 h than [^{161}Tb]Tb-PSMA-617 (39 versus 21; $p < 0.005$) (Fig. 5A). A 24-hour recovery period was included following the 4-hour incubation to assess DNA repair. PC3 PIP cells demonstrated incomplete repair of the induced DNA lesions, with repair rates varying between 10 and 48% (Fig. S15), indicating that the genetic damage induced by the ^{161}Tb-radiocomplexes exceeded the cell's repair capacity.

In vivo studies

μSPECT imaging studies in mice with PCa xenografts

To assess the in vivo targeting efficacy and specificity of the radiocomplexes, SCID/Beige mice implanted with PSMA-negative (PC3 flu; left shoulder) and PSMA-positive (PC3 PIP; right shoulder) tumors were injected with [^{161}Tb]Tb-PSMA-617, [^{161}Tb]Tb-TPP-PSMA and [^{161}Tb]Tb-TPP-G_3-PSMA. A longitudinal SPECT/CT study up to 7 days was performed. The maximum intensity projection (MIP) images and the μSPECT-based SUV data obtained for each radiocomplex are presented in Figs. 6 and 7 and Table S3, respectively.

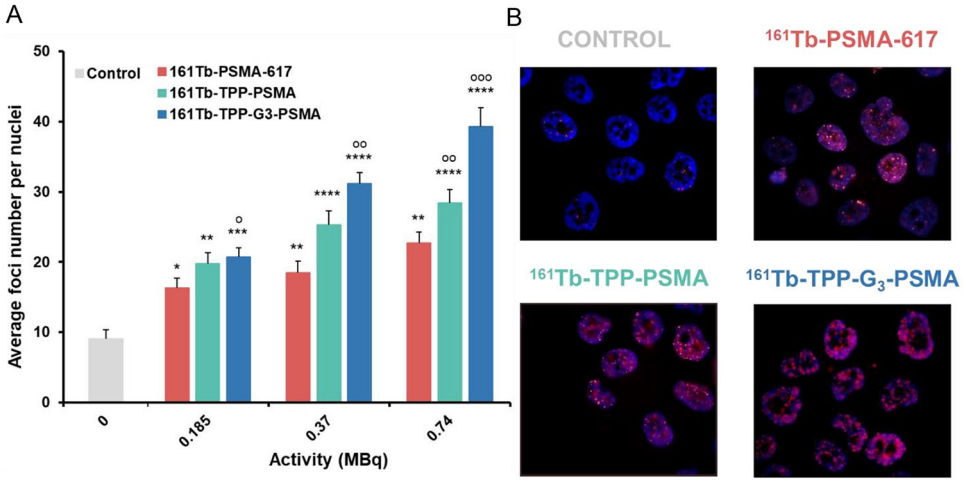


Fig. 5 DNA damage induced by 0.185, 0.37 and 0.74 MBq of [^{161}Tb]Tb-TPP-G3-PSMA, [^{161}Tb]Tb-TPP-PSMA and [^{161}Tb]Tb-PSMA-617 in PC3 PIP cells, after 4 h incubation at 37 °C. Control cells were incubated with medium only. (**A**) Quantification of γ-H_2AX foci per nucleus in PC3 PIP cells (mean ± SEM, 2 independent experiments). Statistical differences compared to the control (0 MBq) are denoted as * $p < 0.05$; ** $p < 0.01$; *** $p < 0.005$; **** $p < 0.001$), compared to [^{161}Tb]Tb-PSMA-617 as $^{o}p < 0.05$; $^{oo}p < 0.01$; $^{ooo}p < 0.005$, and were determined by two-way ANOVA with Tukey's multiple comparisons test. (**B**) Representative fluorescence images of cells exposed to 0.74 MBq for 4 h. γ-H2AX immunostaining highlights DNA damage, while DAPI staining marks the nuclei

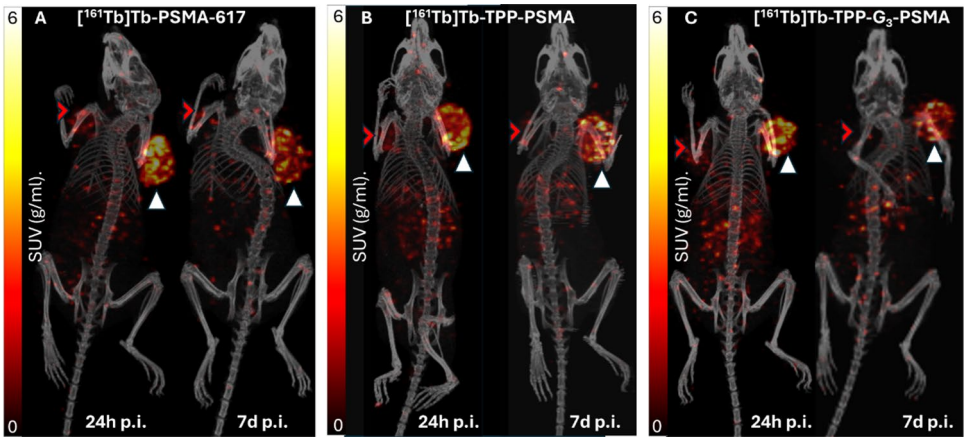


Fig. 6 Fused μSPECT-CT images with maximum intensity projections (MIP) of SPECT at 24 h and 7 days post-injection of one representative mouse from each experimental group: (**A**) [^{161}Tb]Tb-PSMA-617, (**B**) [^{161}Tb]Tb-TPP-PSMA, and (**C**) [^{161}Tb]Tb-TPP-G_3-PSMA. PSMA-positive and PSMA-negative tumors are indicated by a white triangle and a red arrow, respectively

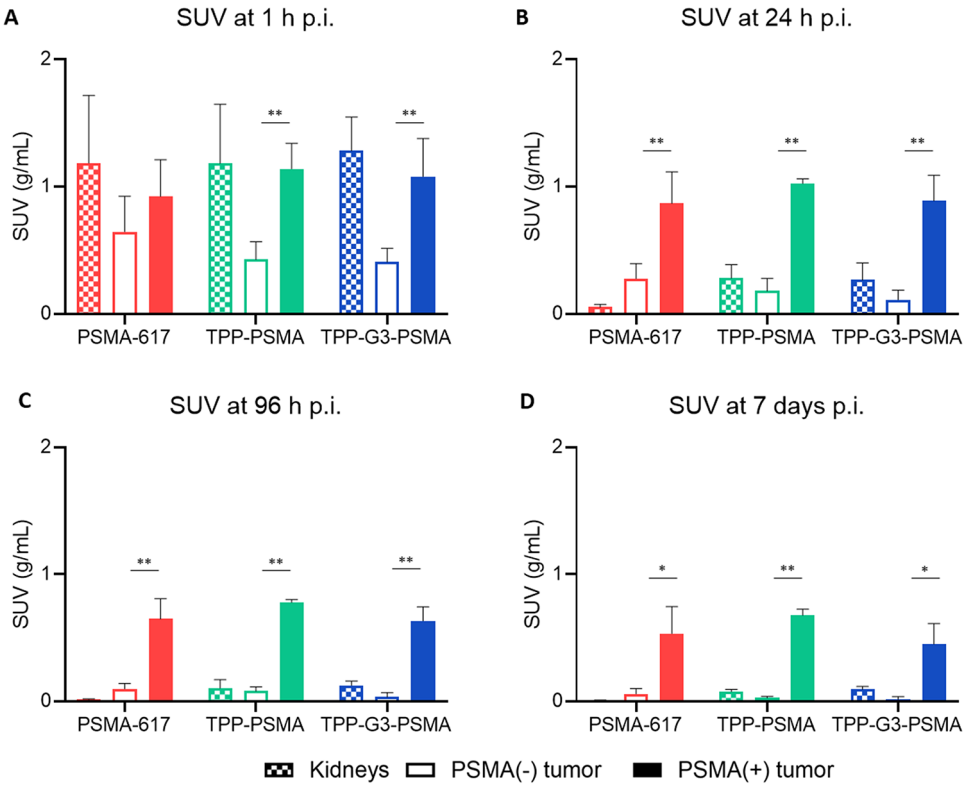


Fig. 7 Comparison of μSPECT-based SUV data of [^{161}Tb]Tb-PSMA-617 (PSMA-617), [^{161}Tb]Tb-TPP-PSMA (TPP-PSMA), [^{161}Tb]Tb-TPP-G_3-PSMA (TPP-G_3-PSMA) at 1 h, 24 h, 96 h, and 7 days p.i. Error bars represent the standard error of the mean (SEM) with $n = 4$ for all groups. Statistical differences were analyzed using an unpaired t-test: PSMA-negative (PC3 Flu) vs. positive (PC3 PIP) tumor uptake (* $p < 0.05$, ** $p < 0.01$)

The single-targeted [^{161}Tb]Tb-PSMA-617 showed substantial uptake in PSMA-positive tumors at 1 h p.i. with a standardized uptake value (SUV) of 0.92 ± 0.29 g/mL. This uptake was sustained over time, with an SUV of 0.53 ± 0.21 g/mL remaining at 7 days p.i., indicating prolonged retention in the target tissue. [^{161}Tb]Tb-PSMA-617 showed similar initial uptake in the kidneys (SUV 1.18 ± 0.53 g/mL) and moderate uptake in

PSMA-negative tumors (SUV 0.65 ± 0.28 g/mL) at 1 h p.i. However, by 24 h p.i., the radiocomplex had largely cleared from the kidneys (SUV 0.05 ± 0.02 g/mL) and PSMA-negative tumors (SUV 0.28 ± 0.12 g/mL), demonstrating efficient clearance from non-target tissues.

Similarly, the TPP-containing dual-targeted complexes [^{161}Tb]Tb-TPP-PSMA and [^{161}Tb]Tb-TPP-G_3-PSMA, demonstrated fast renal clearance and high PSMA-specific tumor uptake comparable to [^{161}Tb]Tb-PSMA-617 up to 7 days p.i. Notably, at 1 h p.i., the dual-targeted complexes showed lower uptake in PSMA-negative tumors (SUV 0.43 ± 0.14 g/mL and 0.41 ± 0.14 g/mL, respectively) compared to [^{161}Tb]Tb-PSMA-617 (SUV 0.65 ± 0.28 g/mL). This reduction suggests that the inclusion of the TPP moiety minimizes non-specific uptake without unduly compromising the pharmacokinetic profile. These findings were corroborated by ex vivo autoradiography at 7 days p.i., which confirmed high PSMA-specific tumor uptake for all PSMA-targeted radiocomplexes (Figure S16).

Evaluation of in vivo stability

The in vivo metabolic stability of [^{161}Tb]Tb-TPP-G_3-PSMA was evaluated by analyzing blood and urine samples collected 10 min p.i. using radio-HPLC. The compound demonstrated excellent stability, with 97.1 ± 4.4% ($n = 4$) and 98.6 ± 1.1% ($n = 3$) of intact [^{161}Tb]Tb-TPP-G_3-PSMA detected in plasma and in urine, respectively (Fig. S17).

Discussion

The dual-targeted constructs [^{161}Tb]Tb-TPP-PSMA and [^{161}Tb]Tb-TPP-G_3-PSMA were synthesized with high radiochemical yield and purity, comparable to the single-targeted constructs [^{161}Tb]Tb-TPP and [^{161}Tb]Tb-PSMA-617 (Figs. S2-S5). All complexes exhibited excellent in vitro stability (Figs. S6-S9). Additionally, [^{161}Tb]Tb-TPP-G_3-PSMA displayed excellent in vivo metabolic stability in both plasma and urine (Figs. S17), confirming that the inclusion of the TPP pharmacophore did not compromise ligand coordination or radiochemical stability.

Both [^{161}Tb]Tb-TPP-PSMA and [^{161}Tb]Tb-TPP-G_3-PSMA displayed efficient and PSMA-specific internalization in PSMA-positive cells (PC3 PIP and LNCaP), with levels comparable to [^{161}Tb]Tb-PSMA-617. Internalization in PC3 PIP cells was almost completely blocked (> 95%) by the structural unrelated PSMA inhibitor 2-PMPA, confirming the PSMA-specific uptake mechanism (Fig. 2). Minimal internalization in PSMA-negative PC3 flu cells further demonstrated that the TPP moiety did not promote non-specific binding.

The TPP-containing complexes showed enhanced mitochondrial uptake in PC3 PIP cells compared to [^{161}Tb]Tb-PSMA-617 (Fig. 3), consistent with previous findings for analogous ^{111}In-radiocomplexes, though the differences were more pronounced with ^{161}Tb-compounds (Santos et al. 2024). Interestingly, mitochondrial targeting remained robust for [^{161}Tb]Tb-TPP-G_3-PSMA, despite its higher cellular efflux rate. This increased efflux is likely attributable to the cleavage of the G_3 linker by cathepsin B, which is overexpressed in cancer cells. The resulting smaller ^{161}Tb-radiocomplex, retaining the TPP moiety but detached from the PSMA unit, is more prone to cellular efflux but maintains high mitochondrial accumulation. The physicochemical properties of the cleaved

complex, including its size, lipophilicity, and pKa, may influence its intramitochondrial distribution (Pala et al. 2020).

Functionally, the TPP-containing complexes demonstrated superior cytotoxicity compared to [^{161}Tb]Tb-PSMA-617, with [^{161}Tb]Tb-TPP-G_3-PSMA demonstrating the greatest cytotoxicity despite its higher efflux rate. This superior activity of the TPP-containing complexes is likely due to their increased mitochondrial accumulation. Notably, [^{161}Tb]Tb-TPP-G_3-PSMA induced the highest levels of γ-H2AX foci per nucleus, with a 2.5- to 5-fold increase compared to control cells, depending on incubation conditions. This DNA damage likely results from nuclear lesions caused by Auger electrons or reactive oxygen species (ROS) generated within mitochondria, highlighting a synergistic radiobiological interplay between mitochondrial dysfunction, nuclear damage, and radiation-induced cell death (Averbeck and Rodriguez-Lafrasse 2021).

Overall, these findings underscore how subtle differences in the subcellular distribution of ^{161}Tb-constructs, particularly their mitochondrial uptake, can significantly influence their cytotoxicity. However, the exact reason for the enhanced cytotoxicity of [^{161}Tb]Tb-TPP-G_3-PSMA compared to [^{161}Tb]Tb-TPP-PSMA remains unclear. This effect may stem from differences in intracellular trafficking, as suggested by the higher efflux rate observed for the former. Such variations could influence the radiobiological effects of the Auger and EC electrons emitted by ^{161}Tb particularly when the radionuclide localizes in organelles other than the mitochondria.

These promising results strongly motivate further studies to elucidate the radiobiological mechanisms underlying the enhanced in vitro activity of [^{161}Tb]Tb-TPP-PSMA and [^{161}Tb]Tb-TPP-G_3-PSMA compared to [^{161}Tb]Tb-PSMA-617.

In vivo, the pharmacokinetics and tumor uptake of [^{161}Tb]Tb-TPP-PSMA and [^{161}Tb]Tb-TPP-G_3-PSMA were similar to those of [^{161}Tb]Tb-PSMA-617, with efficient clearance from non-target tissues, including the kidneys. These findings contrast with previous studies using ^{111}In-radiocomplexes, where TPP inclusion led to much higher kidney uptake (Santos et al. 2024). This discrepancy highlights the significant impact of radionuclide selection on pharmacokinetics and emphasizes the importance of radionuclide-specific optimization in radiopharmaceutical design. Previous studies have reported that the choice of trivalent radiometal (e.g. ^{111}In versus ^{90}Y) markedly influences the biodistribution of isostructural DOTA-based target-specific radioconjugates, though the underlying mechanisms are not fully understood (Nicolas et al. 2017). It has been suggested that the smaller size of In(III) compared to Y(III) increases the likelihood of fluxional processes, which can influence the relative binding affinity to the target protein and, consequently, affect biodistribution. Similar effect can also be expected for In^{3+} and Tb^{3+}, given the larger ionic radius of Tb^{3+}.

All ^{161}Tb-labeled PSMA-targeting constructs showed high and PSMA-specific tumor retention up to 7 days p.i., indicating that the TPP moiety had no negative effect on target binding in vivo. The in vivo stability study showed that [^{161}Tb]Tb-TPP-G_3-PSMA is stable in plasma and urine, indicating that the G_3 linker is not cleaved during circulation or excretion. This observation supports the hypothesis that linker cleavage predominantly occurs within targeted cancer tissues, where cathepsin B is often overexpressed. Such selective cleavage may enhance

mitochondrial targeting by facilitating the accumulation of the smaller cleaved complex within cancer cell mitochondria.

Conclusion

The dual-targeted ^{161}Tb radiocomplexes, integrating PSMA targeting with mitochondrial localization, demonstrated significantly enhanced radiocytotoxicity in PSMA-positive prostate cancer cells by increasing DNA damage compared to the single-targeted PSMA complex. These findings underscore the therapeutic potential of combining mitochondrial-targeting moieties with PSMA-directed radiopharmaceuticals as a novel strategy to improve prostate cancer treatment outcomes. While the successful in vivo tumor targeting and favorable pharmacokinetics highlight the clinical potential of these constructs, further in vivo efficacy studies are required to validate their potential therapeutic benefits. Additionally, continued research is essential to elucidate the radiobiological mechanisms underpinning the enhanced in vitro activity of [^{161}Tb]Tb-TPP-PSMA and [^{161}Tb]Tb-TPP-G_3-PSMA, which may guide the design of next-generation radiopharmaceuticals. To optimize the biological performance of heterobivalent TPP-PSMA ^{161}Tb-radiocomplexes, future investigations should explore structural modifications, such as incorporating more lipophilic TPP moieties (McCluskey et al. 2019) or employing alternative cleavable linkers to enhance the intracellular release of smaller mitochondria-tropic complexes carrying the TPP group (Machulkin et al. 2021; Boinapally et al. 2021).

Supplementary Information

The online version contains supplementary material available at https://doi.org/10.1186/s41181-025-00339-6.

Supplementary Material 1

Supplementary Material 2

Acknowledgements

PC3 human prostate cancer cell line, PSMA-positive 16 (PSMA+) PC3 PIP and PSMA-negative (PSMA-) PC3 flu cells, were kindly provided by Prof. Dr. Martin 17 Pomper (Johns Hopkins University School of Medicine, Baltimore, MD, USA).

Author contributions

JFS: Experimental design, radiolabeling, in vitro experiments and in vivo experiments, data analysis. Original draft preparation, review and editing of the manuscript. CVL: Experimental design, radiolabeling, in vitro experiments and in vivo experiments, data analysis. Original draft preparation, review and editing of the manuscript. CDS: Radiolabeling, in vitro experiments, data analysis. Review and editing of the manuscript. IC: Radiolabeling, in vitro experiments, data analysis. Review and editing of the manuscript. CF: Experimental design, chemistry, radiolabeling, data analysis. Review and editing of the manuscript. PR: In vitro experiments, data analysis. Review and editing of the manuscript. AB: In vitro experiments, data analysis. Review and editing of the manuscript. CIGP: In vitro experiments, data analysis. Review and editing of the manuscript. FM: Experimental design, in vitro experiments, data analysis. Review and editing of the manuscript. CC: In vivo experiments and data analysis. Review and editing of the manuscript. MO: Experimental design, data analysis. Review and editing of the manuscript. MVV: Experimental design, data analysis. Review and editing of the manuscript. FC: Experimental design, radiolabeling, in vitro experiments and in vivo experiments, data analysis. Original draft preparation, review and editing of the manuscript. AP: Experimental design, data analysis. Original draft preparation, review and editing of the manuscript. All authors read and approved the final manuscript.

Funding

This work was supported by Fundação para a Ciência e Tecnologia, Portugal (projects UID/Multi/04349/2020 and PTDC/MED-QUI/1554/2020 and PhD fellowships 2020.07119.BD to CIGP, PRT/BD/154612/2023 to JFS and PRT/BD/154625/2023 to CDS), and received funding from Research Foundation-Flanders (FWO) and the European Union's Horizon 2020 research and innovation program under grant agreement No 101008571 (PRISMAP – The European medical radionuclides program). The IAEA Coordinated Research Project F22078 is also acknowledged.

Data availability

The raw data presented in this study are available on request from the corresponding author.

Declarations

Ethics approval and consent to participate
In vivo experiments were approved by the KU Leuven ethical review board and conducted in accordance with the Belgian and EU law of animal protection.

Consent for publication
Not applicable.

Competing interests
All the authors declare no competing interests.

Received: 7 January 2025 / Accepted: 27 March 2025
Published online: 11 April 2025

References

Antczak C, Jaggi JS, LeFave CV, Curcio MJ, McDevitt MR, Scheinberg DA. Influence of the linker on the biodistribution and catabolism of Actinium-225 Self-Immolative Tumor-Targeted isotope generators. Bioconjug Chem. 2006;17:1551–60.
Averbeck D, Rodriguez-Lafrasse C. Role of mitochondria in radiation responses: epigenetic, metabolic, and signaling impacts. Int J Mol Sci. 2021;22:11047.
Boinapally S, Ahn H-H, Cheng B, Brummet M, Nam H, Gabrielson KL, et al. A prostate-specific membrane antigen (PSMA)-targeted prodrug with a favorable in vivo toxicity profile. Sci Rep. 2021;11:7114.
Bolcaen J, Gizawy MA, Terry SYA, Paulo A, Cornelissen B, Korde A, et al. Marshalling the potential of Auger electron radiopharmaceutical therapy. J Nucl Med. 2023;64:1344–51.
Borgna F, Haller S, Rodriguez JMM, Ginj M, Grundler PV, Zeevaart JR, et al. Combination of terbium-161 with somatostatin receptor antagonists—a potential paradigm shift for the treatment of neuroendocrine neoplasms. Eur J Nucl Med Mol Imaging. 2022;49:1113–26.
Cassells I, Ahenkorah S, Burgoyne AR, Van de Voorde M, Deroose CM, Cardinaels T, et al. Radiolabeling of human serum albumin with Terbium-161 using mild conditions and evaluation of in vivo stability. Front Med. 2021;8:675122.
Collins SM, Gilligan C, Pierson B, Ramirez N, Goodwin M, Pearce AK, et al. Determination of the ^{161}Tb half-life. Appl Radiat Isot. 2022;182:110140.
Favaretto C, Grundler PV, Talip Z, Landolt S, Sepini L, Köster U, et al. ^{161}Tb-DOTATOC production using a fully automated disposable cassette system: A first step toward the introduction of ^{161} Tb into the clinic. J Nucl Med. 2023;64:1138–44.
Fernandes C, Palma E, Silva F, Belchior A, Pinto CIG, Guerreiro JF, et al. Searching for a paradigm shift in Auger-Electron cancer therapy with Tumor-Specific radiopeptides targeting the mitochondria and/or the cell nucleus. Int J Mol Sci. 2022;23:7238.
Figueiredo D, Fernandes C, Silva F, Palma E, Raposinho P, Belchior A, et al. Synthesis and biological evaluation of ^{99m}Tc(I) Tricarbonyl complexes Dual-Targeted at tumoral mitochondria. Molecules. 2021;26:441.
Holzleitner N, Cwojdzinski T, Beck R, Urtz-Urban N, Hillhouse CC, Grundler PV, et al. Preclinical evaluation of Gastrin-Releasing peptide receptor antagonists labeled with ^{161} Tb and ^{177} Lu: A comparative study. J Nucl Med. 2024;65:481–4.
Larouze A, Alcocer-Ávila M, Morgat C, Champion C, Hindié E. Membrane and nuclear absorbed doses from ^{177}Lu and ^{161}Tb in tumor clusters: effect of cellular heterogeneity and potential benefit of dual Targeting—A Monte Carlo study. J Nucl Med. 2023;64:1619–24.
Machulkin AE, Uspenskaya AA, Zyk NU, Nimenko EA, Ber AP, Petrov SA, et al. Synthesis, characterization, and preclinical evaluation of a Small-Molecule Prostate-Specific membrane Antigen-Targeted monomethyl auristatin E conjugate. J Med Chem. 2021;64:17123–45.
McCluskey SP, Haslop A, Coello C, Gunn RN, Tate EW, Southworth R, et al. Imaging of Chemotherapy-Induced acute cardiotoxicity with ^{18}F-Labeled lipophilic cations. J Nucl Med. 2019;60:1750–6.
Müller C, Umbricht CA, Gracheva N, Tschan VJ, Pellegrini G, Bernhardt P, et al. Terbium-161 for PSMA-targeted radionuclide therapy of prostate cancer. Eur J Nucl Med Mol Imaging. 2019;46:1919–30.
Nicolas GP, Mansi R, McDougall L, Kaufmann J, Bouterfa H, Wild D, et al. Biodistribution, pharmacokinetics, and dosimetry of ^{177}Lu-, ^{90}Y-, and ^{111}In-Labeled somatostatin receptor antagonist OPS201 in comparison to the agonist ^{177}Lu-DOTATATE: the mass effect. J Nucl Med. 2017;58:1435–41.
Pala L, Senn HM, Caldwell ST, Prime TA, Warrington S, Bright TP, et al. Enhancing the mitochondrial uptake of phosphonium cations by carboxylic acid incorporation. Front Chem. 2020;8:783.
Rasul S, Hacker M, Kretschmer-Chott E, Leisser A, Grubmüller B, Kramer G, et al. Clinical outcome of standardized ^{177}Lu-PSMA-617 therapy in metastatic prostate cancer patients receiving 7400 MBq every 4 weeks. Eur J Nucl Med Mol Imaging. 2020;47:713–20.
Rogakou EP, Pilch DR, Orr AH, Ivanova VS, Bonner WM. DNA Double-stranded breaks induce histone H2AX phosphorylation on Serine 139. J Biol Chem. 1998;273:5858–68.
Ruigrok EAM, Van Weerden WM, Nonnekens J, De Jong M. The future of PSMA-Targeted radionuclide therapy: an overview of recent preclinical research. Pharmaceutics. 2019;11:560.
Santos JF, Braz MT, Raposinho P, Cleeren F, Cassells I, Leekens S, et al. Synthesis and preclinical evaluation of PSMA-Targeted ^{111}In-Radioconjugates containing a Mitochondria-Tropic triphenylphosphonium carrier. Mol Pharm. 2024;21:216–33.
Spoormans K, Struelens L, Vermeulen K, De Saint-Hubert M, Koole M, Crabbé M. The emission of internal conversion electrons rather than Auger electrons increased the Nucleus-Absorbed dose for ^{161}Tb compared with ^{177}Lu with a higher dose response for [^{161}Tb]Tb-DOTA-LM3 than for [^{161}Tb]Tb-DOTATATE. J Nucl Med. 2024;65:1619–25.
Tschan VJ, Busslinger SD, Bernhardt P, Grundler PV, Zeevaart JR, Köster U, et al. Albumin-Binding and conventional PSMA ligands in combination with ^{161}Tb: biodistribution, dosimetry, and preclinical therapy. J Nucl Med. 2023;64:1625–31.
Van Laere C, Koole M, Deroose CM, De Voorde MV, Baete K, Cocolios TE, et al. Terbium radionuclides for theranostic applications in nuclear medicine: from atom to bedside. Theranostics. 2024;14:1720–43.

Xie Z, Zhao M, Yan C, Kong W, Lan F, Narengaowa, et al. Cathepsin B in programmed cell death machinery: mechanisms of execution and regulatory pathways. Cell Death Dis. 2023;14:255.
Zielonka J, Joseph J, Sikora A, Hardy M, Ouari O, Vasquez-Vivar J, et al. Mitochondria-Targeted Triphenylphosphonium-Based compounds: syntheses, mechanisms of action, and therapeutic and diagnostic applications. Chem Rev. 2017;117:10043–120.

Publisher's note

Springer Nature remains neutral with regard to jurisdictional claims in published maps and institutional affiliations.